

# Two-Switch Voltage Equalizer Using an LLC Resonant Inverter and Voltage Multiplier for Partially-Shaded Series-Connected Photovoltaic Modules

Masatoshi Uno, *Member, IEEE*, and Akio Kukita

**Abstract**— Various kinds of differential power processing (DPP) converters and voltage equalizers have been proposed for series-connected photovoltaic (PV) modules to prevent negative influences of partial shading, such as significant reduction in power generation and the occurrence of multiple maximum power points (MPPs), including local and global MPPs, that hinders and confuses MPP tracking algorithms to operate properly. However, since conventional topologies are based on multiple individual dc-dc converters, the required switch count increases proportionally to the number of modules connected in series, increasing the complexity. A two-switch voltage equalizer using an LLC resonant inverter and voltage multiplier is proposed in this paper. The circuitry can be dramatically simplified compared with conventional topologies thanks to the two-switch configuration. Detailed operation analyses for the LLC resonant inverter and voltage multiplier are separately performed. Experimental equalization tests emulating partially-shaded conditions were performed for four PV modules connected in series. With the proposed voltage equalizer, local MPPs successfully disappeared and extractable maximum powers increased compared to those without equalization, demonstrating the effectiveness and performance of the proposed voltage equalizer.

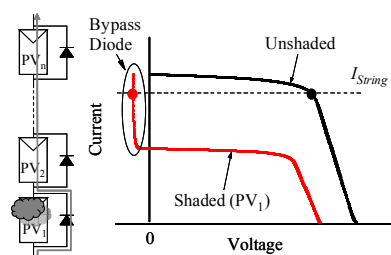
**Index Terms**— LLC resonant inverter, partial shading, photovoltaic system, voltage equalizer, voltage multiplier.

## I. INTRODUCTION

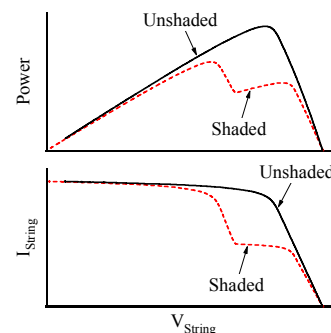
Partial shading on a photovoltaic (PV) string comprising multiple PV modules/substrings (hereafter, simply called modules) connected in series causes a significant characteristic mismatch among modules; shaded modules are generally less capable of generating current due to reduced irradiance. If shaded modules are incapable of a string current, they are bypassed and the string current circumvents through the bypass diode, as shown in Fig. 1(a), which means shaded and unshaded

modules in a string are operated at totally different voltage levels. The characteristic mismatch due to partial shading is well known as triggering not only significantly reduced power generation but also multiple maximum power points (MPPs), including one global MPP and local MPP(s), as shown in Fig. 1(b). The existence of multiple MPPs confuses and hinders the conventional MPP tracking (MPPT) algorithm to extract maximum power. Although advanced MPPT algorithms have been proposed, with which a global MPP can be found by sweeping operation voltage over a wide range and tracked even under partially-shaded conditions, a significant reduction in power generation due to the bypassed shaded modules is inevitable.

In decentralized power management for PV systems, micro-converters or -inverters have been introduced as module-level power converters. Since each individual PV module is controlled by a module-level micro inverter/converter, issues on partial shading are resolved [1], [2]. However, increased cost and complexity due to multiple



(a) Current path and module characteristics.



(b) String characteristics.

Fig. 1. PV string under partially-shaded condition: (a) current path and module characteristics, (b) string characteristics.

Manuscript received January 8, 2014, revised April 7, 2014; accepted June 29, 2014. This work was supported in part by the Ministry of Education, Culture, Sports, Science, and Technology through Grant-in-Aid for Young Scientists (B) 25820118.

Copyright (c) 2011 IEEE. Personal use of this material is permitted. However, permission to use this material for any other purposes must be obtained from the IEEE by sending a request to pubs-permissions@ieee.org.

The authors are with Japan Aerospace Exploration Agency, Ibaraki 305-8505, Japan (e-mail: uno.masatoshi@jaxa.jp; kukita.akio@jaxa.jp).

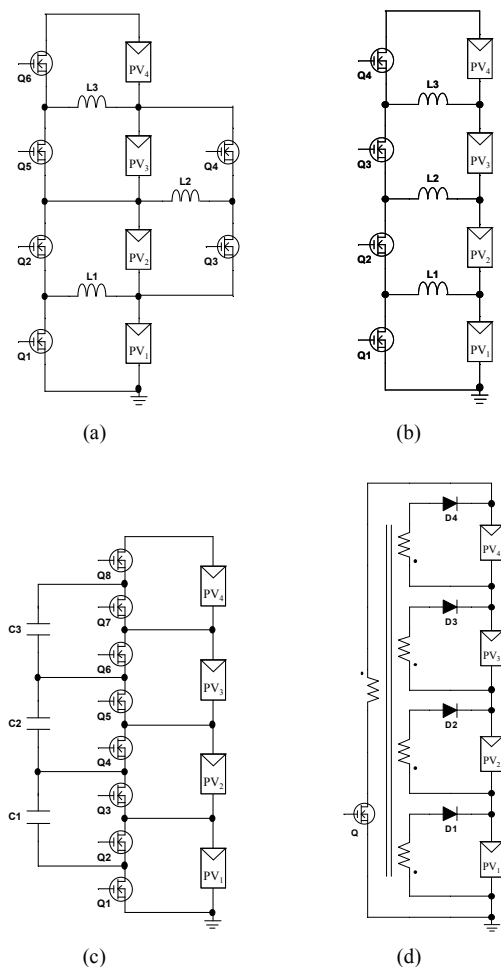


Fig. 2. Conventional differential power processing converters and voltage equalizers based on (a) buck-boost converter, (b) multi-stage buck-boost converter, (c) switched capacitor converter, and (d) multi-winding flyback converter.

micro-inverters/converters are very likely. In addition, the lower power utilization due to the efficiency penalty of the added power conversion stage is also considered a major drawback [3], [17].

Various kinds of differential power processing (DPP) converters and voltage equalizers have been proposed and developed to address issues on partial shading in series-connected PV modules [2]–[24]. These converters transfer part of the generated power of unshaded PV modules to shaded modules so that all the individual PV modules connected in series can operate at virtually the same voltage or even each MPP. With DPP converters or voltage equalizers, an efficient central converter/inverter can be used without suffering from the partial shading issues, hence increasing total power conversion efficiency and decreasing system cost and complexity compared with conventional decentralized systems requiring multiple module-level converters/inverters.

The basic concept and circuit topologies of conventional DPP converters and voltage equalizers are very similar to cell voltage equalizers used for series-connected energy storage cells, such as lithium-ion batteries and supercapacitors; these

equalizers are based on buck-boost converters [25]–[28], switched capacitor converters [29]–[33], flyback converters [34], [35] and multi-winding flyback/forward converters [36]–[38], etc. [39], [40]. Representative DPP converters and voltage equalizers are listed in Fig. 2. Most conventional topologies are based on individual multiple bidirectional dc-dc converters such as buck-boost converters [3]–[10] (and some extended topologies [11]–[14]), multi-stage buck-boost converters [15], [16], and switched capacitor converters [17], [18], shown in Figs. 2(a)–(c), respectively. Since the power transfer in these topologies is limited to two adjacent modules, the generated power of unshaded modules may have to traverse multiple converters and modules (especially when numerous modules are connected in series) before reaching the shaded module, collectively decreasing efficiency [14]. In addition, the number of switches required is proportional to the number of modules connected in series, which means complexity tends to soar, since each switch requires a driver IC and several auxiliary devices including passive components and opto-coupler. With bidirectional flyback converters [19]–[23], power transfer between a shaded module and string is feasible, but multiple transformers are required, as well as multiple switches.

In the multi-winding flyback converter [24], shown in Fig. 2(d), the number of switches can be minimized. However, it is known that the transformer needs to be designed so that parameters of multiple secondary windings are tightly matched. Accordingly, the transformer design tends to become more complex with an increasing number of modules connected in series [39], [40]. Modularity, or extendibility, is not good because the multi-winding transformer needs to be redesigned without impairing parameter matching when the number of modules connected in series changes.

In this paper, a two-switch voltage equalizer using an LLC resonant inverter and voltage multiplier is proposed for partially-shaded series-connected PV modules. The two-switch configuration can dramatically simplify the circuitry compared to conventional DPP converters or voltage equalizers. A representative circuit description is introduced, and the major benefits of the proposed voltage equalizer are discussed in Section II. Detailed operation analyses for the LLC resonant inverter and voltage multiplier are separately performed in Section III, followed by derivation for a dc equivalent circuit of the proposed voltage equalizer. Power distribution scenario with the proposed voltage equalizer under a partially-shaded condition is discussed in Section IV. Major losses in the voltage equalizer are modeled in Section V, while in Section VI, experimental equalization tests emulating partially-shaded conditions are performed for four PV modules connected in series, and the experimental results are compared with simulation results of the derived dc equivalent circuit.

## II. TWO-SWITCH VOLTAGE EQUALIZER USING AN LLC RESONANT INVERTER AND VOLTAGE MULTIPLIER

### A. Circuit Description

The proposed voltage equalizer is basically a combination of

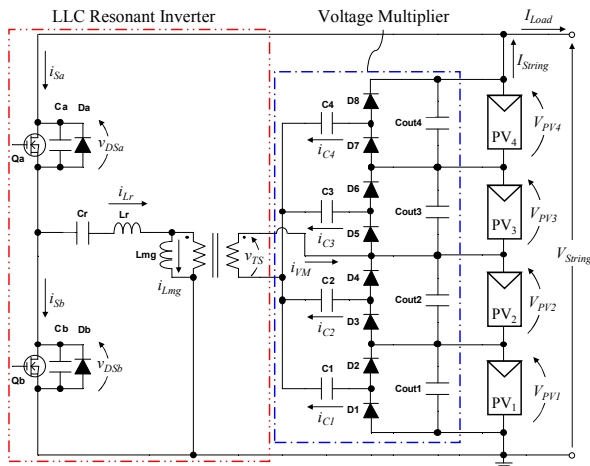


Fig. 3. Two-switch voltage equalizer using an LLC resonant inverter with voltage multiplier for four PV modules connected in series.

an LLC resonant inverter and voltage multiplier, as shown in Fig. 3, which illustrates an example configuration for four PV modules ( $PV_1$ – $PV_4$ ) connected in series.  $C_a$ – $C_b$  and  $D_a$ – $D_b$  in the LLC inverter are the parasitic output capacitances and body diodes of the MOSFETs  $Q_a$ – $Q_b$ , respectively. The voltage multiplier is composed of energy transfer capacitors  $C_1$ – $C_4$  and diodes  $D_1$ – $D_8$ . The series-connected PV modules are tied to the input of the LLC inverter, and the individual outputs of the voltage multiplier are connected to each PV module. The LLC inverter is powered by the series connection of  $PV_1$ – $PV_4$  and produces an ac voltage/current wave at its output (i.e. at the transformer secondary winding). The voltage multiplier is driven by the ac wave generated by the LLC inverter and theoretically produces uniform voltages at each output. The voltage multiplier preferentially supplies power to a module with the lowest voltage among  $PV_1$ – $PV_4$ . In other words, the series connection of  $PV_1$ – $PV_4$  provides power for a module having the lowest voltage through the proposed voltage equalizer. In general, an operation voltage of a shaded module tends to be lower than that of unshaded modules when they are connected in series, as mentioned in Section I. Accordingly, the proposed voltage equalizer operates so that all series-connected PV modules support and provide power for a shade module.

Although one side of the transformer secondary winding is connected to the mid-point of the voltage multiplier in Fig. 3, it can be tied to other junction points in the stacked  $C_{out1}$ – $C_{out4}$  (including the ground). Since an average voltage of a transformer winding under a steady-state condition is zero, the mid-point of the stacked  $C_{out1}$ – $C_{out4}$  is the best place in terms of reducing voltage rating of  $C_1$ – $C_4$ . The average voltage of  $C_4$ , for example, is equal to  $V_{PV3} + V_{PV4}/2$  in the case of Fig. 3—odd- and even-numbered diodes in the voltage multiplier alternately conduct with the same duty cycle, as will be shown in Fig. 5, and hence, only a half of  $V_{PV4}$  is applied to  $C_4$ . On the other hand, if the secondary winding is tied to the junction of  $C_{out1}$  and  $C_{out2}$ , the average voltage of  $C_4$  is increased to  $V_{PV2} + V_{PV3} + V_{PV4}/2$ .

The number of PV modules connected in series can be arbitrary extended by adding capacitors and diodes in the

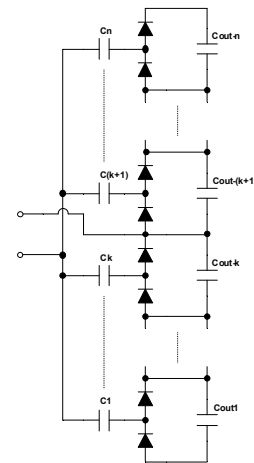


Fig. 4. Voltage multiplier generalized for  $n$  PV modules connected in series.

voltage multiplier. The voltage multiplier generalized for  $n$  modules connected in series is shown in Fig. 4, in which the LLC resonant inverter and series-connected PV modules are not illustrated for the sake of simplicity. The junction of  $C_{out-k}$  and  $C_{out-(k+1)}$  it is tied to the secondary winding. From the perspective of voltage rating of  $C_1$ – $C_n$ , the junction of  $C_{out-k}$  and  $C_{out-(k+1)}$  should be the mid-point. If  $n$  is an odd number and there is no mid-point, the best design effort is  $k \approx n/2$ .

### B. Major Benefits and Comparison with Conventional Topologies

In general, each switch requires ancillary components, including a gate driver IC and its power supply, and several passive components, and therefore, the switch count is considered a good index to represent the circuit complexity. Only two switches are necessary for the proposed voltage equalizer, regardless of the number of modules connected in series, significantly simplifying the circuitry compared to conventional DPP converters and voltage equalizers based on multiple dc-dc converters shown in Figs. 2(a)–(c)—switches in Figs. 2(a)–(c) cannot be replaced with diodes because these converters must be bidirectional. The reduced switch count is the most prominent benefit of the proposed voltage equalizer, whereas diode conduction loss that naturally becomes the most predominant loss factor (as will be shown in Fig. 17) would be a drawback.

The conventional topologies shown in Figs. 2(a)–(c) offer the best modularity, as they can be arbitrary extended by increasing the number of converters. Meanwhile, the proposed voltage equalizer needs to be redesigned by adding capacitors and diodes, and adjusting component voltage/current rating and transformer turns ratio. However, its modularity is considered fair compared to that of the equalizer shown in Fig. 2(d) because of lack of a multi-winding transformer; the parameter matching requirement for multiple secondary windings is the most cumbersome issue that impairs the modularity [39], [40].

As briefly mentioned in Section I, the power transfer in the conventional topologies shown in Figs. 2(a)–(c) is limited only

between two adjacent modules, and hence, the collective power conversion loss might be significant, depending on partial-shading conditions and the number of modules connected in series [14]. For example, in the case that the  $PV_1$  in Fig. 2(a) is partially-shaded, powers from  $PV_2$ – $PV_4$  have to traverse one, two, and three DPP converters, respectively, before reaching  $PV_1$ . With the proposed voltage equalizer, on the other hand, the power from the string can be directly transferred to  $PV_1$ , reducing the number of power conversions.

The proposed voltage equalizer is operable with open-loop control and operating voltages of PV modules are automatically nearly unified by the proposed equalizer, even at a fixed duty cycle and fixed frequency. This means the feedback loop and control circuit can be eliminated, further simplifying the circuitry; details of which will be discussed in Section III.

With the DPP converters based on buck-boost converters shown in Figs. 2(a) and (b), by properly controlling duty cycles, each individual PV module can operate at its MPP, even when partial shading occurs [5], [6], [15], [16]. However, control for individual MPPT tends to be complex because the duty cycle for each DPP converter needs to be individually controlled according to shading conditions. With the proposed equalizer, conversely, the operation voltages of series-connected modules cannot be individually controlled, similar to voltage equalizers based on switched capacitor converters, because the voltage multiplier in the proposed voltage equalizer comprises solely passive components. The proposed voltage equalizer operates so that all operating voltages of modules become nearly uniform (as will be experimentally demonstrated in Section VI), indicating the individual MPPT is unfeasible; dc equivalent circuits (Figs. 8 and 11), which will be derived in the following section, would better explain how module voltages are equalized under partially-shaded conditions. Although individual MPPT is not feasible with the proposed voltage equalizer, equalizing module voltages simply would be beneficial enough when considering MPP voltages relatively insensitive to shading conditions compared to currents [17], [21], [22].

### III. OPERATING ANALYSIS

#### A. Key Waveforms and Current Flow Directions

Similar to conventional LLC resonant inverters, the LLC inverter in the proposed voltage equalizer is operated between two resonant angular frequencies of  $\omega_r$  and  $\omega_0$ ,

$$\frac{1}{\sqrt{L_r C_r}} = \omega_r \geq \omega \geq \omega_0 = \frac{1}{\sqrt{(L_r + L_{mg}) C_r}}, \quad (1)$$

where  $\omega$  is the angular switching frequency,  $L_r$  and  $L_{mg}$  are the inductances of the resonant inductor  $L_r$  (or the leakage inductance of the transformer) and magnetizing inductor  $L_{mg}$ , and  $C_r$  is the capacitance of the resonant capacitor  $C_r$ . As will be discussed in Section III-C, the proposed voltage equalizer is designed to satisfy  $L_{mg} \gg L_r$  and is operated at  $\omega_r > \omega \gg \omega_0$ .

Here, the case that  $PV_1$  is partially shaded is taken as an example to explain the fundamental operation of the proposed

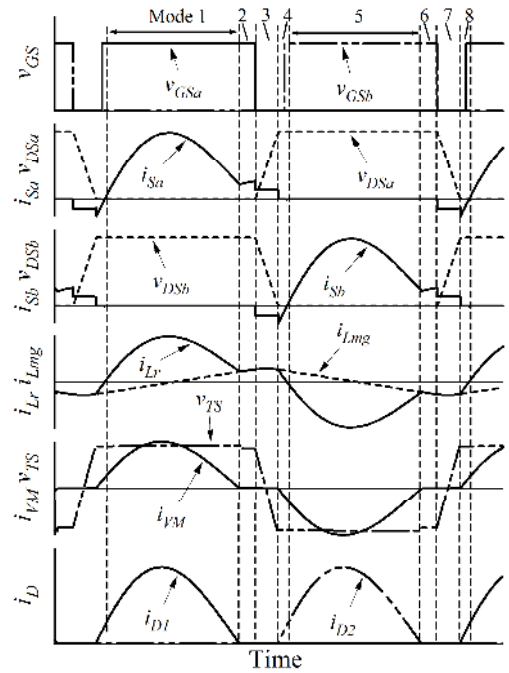


Fig. 5. Key operation waveforms when  $PV_1$  is shaded.

voltage equalizer. Key operation waveforms and current flow directions when  $PV_1$  is partially-shaded and its voltage  $V_{PV1}$  is the lowest among  $V_{PV1}$ – $V_{PV4}$  are shown in Figs. 5 and 6, respectively. Switches  $Q_a$  and  $Q_b$  are alternately driven at a fixed duty cycle of just under 50%. Figure 6 is illustrated assuming that currents in the voltage multiplier are buffered by smoothing capacitors.

In Mode 1,  $L_r$  and  $C_r$  resonate and the current of  $L_r$ ,  $i_{Lr}$ , sinusoidally changes, whereas the current of  $L_{mg}$ ,  $i_{Lmg}$ , linearly increases. In the voltage multiplier, the odd-numbered diode,  $D_1$ , conducts to charge  $C_1$ , and currents in the voltage multiplier ( $i_{VM}$  and  $i_{D1}$ ) are also sinusoidal waves. The next mode, Mode 2, begins when  $i_{Lr}$  and  $i_{Lmg}$  become the same. In Mode 2,  $L_{mg}$  starts participating in the resonance but  $i_{Lmg}$  can be assumed to increase linearly because of  $\omega \gg \omega_0$ . Both  $i_{Lr}$  and  $i_{Lmg}$  linearly increase at the same rate, while no current flows in the voltage multiplier. By removing the gating signal of  $v_{GSa}$ ,  $Q_a$  is turned off at zero voltage, achieving zero-voltage switching (ZVS), and the operation moves to Mode 3, in which  $L_{mg}$  and  $C_a$ – $C_b$  resonate. Despite the resonance,  $i_{Lmg}$  can be assumed constant provided that the total capacitance of  $C_a$ – $C_b$  is negligibly small compared to  $C_r$ .  $C_a$  and  $C_b$  are charged and discharged, respectively, by  $i_{Lmg}$ , and voltages of  $Q_a$  and  $Q_b$ ,  $v_{DSa}$  and  $v_{DSb}$ , rise and fall, respectively. As  $v_{DSa}$  and  $v_{DSb}$  reach  $V_{String}$  (i.e. the sum of  $V_{PV1}$ – $V_{PV4}$ , or the input voltage of the LLC inverter) and zero, respectively, the voltage equalizer starts operating in Mode 4, in which  $i_{Lr}$  is freewheeling through  $D_b$ . At the same time, the even-numbered diode,  $D_2$ , starts conducting to discharge  $C_1$  in the voltage multiplier. As  $i_{Lr}$  decreases and becomes negative, the operation moves to Mode 5, in which  $D_b$  ceases to conduct and  $i_{Lr}$  starts flowing through the channel of  $Q_b$ , achieving zero-voltage and zero-current switching

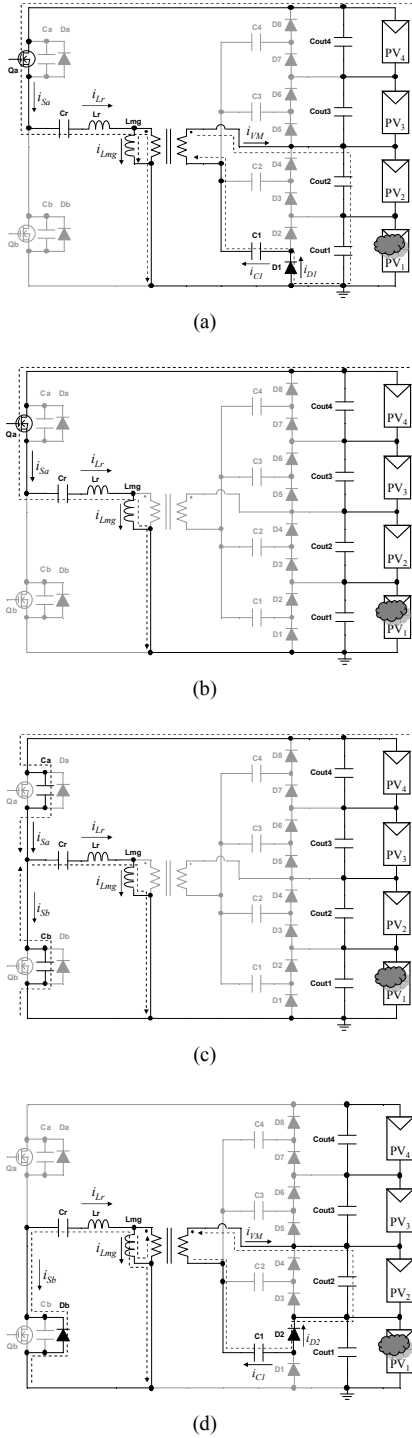


Fig. 6. Current flow directions when PV<sub>1</sub> is shaded in Modes (a) 1, (b) 2, (c) 3, and (d) 4.

(ZVZCS). Modes 5–8 are symmetrical to Modes 1–4.

As shown in Fig. 6, only D<sub>1</sub>, D<sub>2</sub>, and C<sub>1</sub> that are connected to the shaded module of PV<sub>1</sub> are in operation. This operation can be extended to a general case; currents in the voltage multiplier flow through capacitors and diodes that are connected to shaded modules.

### B. Voltage Multiplier

The configuration of the voltage multiplier varies with the number of PV modules, as shown in Fig. 4. In this subsection, a voltage multiplier for two PV modules, PV<sub>j</sub> and PV<sub>k</sub>, shown in Fig. 7, is considered and its operation is generalized so that it can be extended to the case of  $n$  modules connected in series.

As shown in Fig. 5, currents in the voltage multiplier (i.e.  $i_{VM}$  and  $i_D$ ) flow during Modes 1, 4, 5, and 8, while no current flows in the remaining operation modes. By neglecting these inactive operation modes, in which no current flows in the voltage multiplier, the secondary winding voltage  $v_{TS}$  can be approximated as a square wave voltage. Since odd- and even-numbered diodes in the voltage multiplier alternately conduct, voltages at the junctions of diode pairs are also square wave voltages. Based on the fundamental harmonics approximation (FHA), square wave voltages in the voltage multiplier can be transformed into sinusoidal waves, as shown in Fig. 7, where  $v_j$  and  $v_k$  are voltages of diodes D<sub>(2j-1)</sub> and D<sub>(2k-1)</sub> relative to ground level. The voltages of  $v_{TS}$ ,  $v_j$  and  $v_k$  as well as those amplitudes  $V_{m-TS}$ ,  $V_{m-j}$  and  $V_{m-k}$ , are expressed as

$$\begin{cases} v_{TS} = V_{m-TS} \sin \omega_r t = \frac{2}{\pi} V_{TS} \sin \omega_r t \\ v_j = V_{m-j} \sin \omega_r t = \frac{2}{\pi} (V_{PVj} + 2V_D) \sin \omega_r t \\ v_k = V_{m-k} \sin \omega_r t = \frac{2}{\pi} (V_{PVk} + 2V_D) \sin \omega_r t \end{cases} \quad (2)$$

where  $V_{PVj}$  and  $V_{PVk}$  are the voltages of PV<sub>j</sub> and PV<sub>k</sub>, respectively, and  $V_D$  is the forward voltage drop of diodes. Since  $v_j$  and  $v_k$  in (2) are expressed in the identical form, they can be generalized as

$$v_i = V_{m-i} \sin \omega_r t = \frac{2}{\pi} (V_{PVi} + 2V_D) \sin \omega_r t, \quad (3)$$

where  $i$  is the arbitrary integer number (i.e.  $i = 1 \dots n$ ).

$v_{TS}$  and  $v_i$  are in the same phase, and hence, the amplitude of the capacitor current  $i_{Ci}$  and the secondary winding current  $i_{VM}$ ,  $I_{m-Ci}$  and  $I_{m-VM}$ , can be yielded as

$$\begin{cases} I_{m-Ci} = \frac{V_{m-TS} - V_{m-i}}{\sqrt{r_i^2 + \left(\frac{1}{\omega_r C_i}\right)^2}} = \frac{2}{\pi} \frac{V_{TS} - (V_{PVi} + 2V_D)}{\sqrt{r_i^2 + \left(\frac{1}{\omega_r C_i}\right)^2}} \\ I_{m-VM} = \sum_i I_{m-Ci} \end{cases} \quad (4)$$

where  $r_i$  is the ESR of  $C_i$ .

The average current flowing over  $C_i$ ,  $I_{Ci}$ , is expressed as

$$I_{Ci} = \frac{1}{T_S} \int_0^{0.5T_r} I_{m-Ci} \sin \omega_r t dt = \frac{\omega}{\omega_r} \frac{I_{m-Ci}}{\pi}, \quad (5)$$

where  $T_S$  and  $T_r (= 2\pi/\omega_r)$  are the switching and resonant periods, respectively.

Substituting (4) into (5) produces

$$V_{TS} - (V_{PVi} + 2V_D) = I_{Ci} R_{eq-i}, \quad (6)$$

where

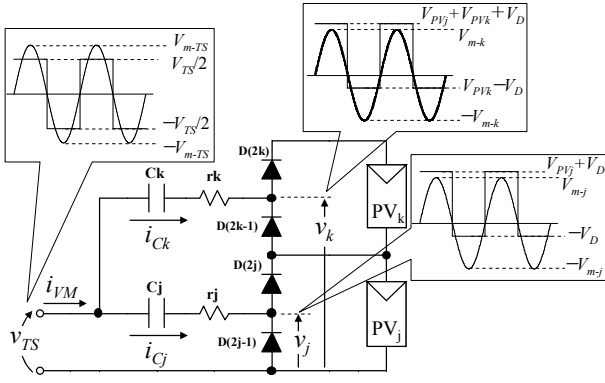


Fig. 7. Square wave voltage and approximated sinusoidal waves in voltage multiplier.

$$R_{eq-i} = \frac{\omega_r}{\omega} \frac{\pi^2}{2} \sqrt{r_i^2 + \left(\frac{1}{\omega_r C_i}\right)^2}. \quad (7)$$

From (6), a dc equivalent circuit of the voltage multiplier for  $n$  modules can be derived, as shown in Fig. 8. All the modules are connected to a common terminal of voltage  $V_{TS}$  through two diodes and one equivalent resistor  $R_{eq-i}$ , and receive currents of  $I_{Ci}$ . In general, voltages of shaded modules tend to be lower than those of unshaded modules provided they are in the same string, as mentioned in Section I. The derived dc equivalent circuit indicates that if the voltages of modules are nonuniform, the voltage equalizer preferentially supplies current for the module with the lowest voltage in the string so that all module voltages become nearly uniform. Although  $R_{eq-i}$  is expressed as resistance in the “dc equivalent” circuit, it is actually impedance, rather than fully dissipative resistance, as expressed by (7).

### C. LLC Resonant Inverter

The proposed voltage equalizer should be designed to consume minimal power when not needed (i.e. when there is no partial shading). In other words, power consumption at no load, or light load efficiency, is an important factor to minimize the no-load loss in the equalizer. Traditional LLC resonant converters are generally designed so that the ratio of  $L_{mg}/L_r$  is about 5 to obtain the desired gain-frequency characteristic, with which an output voltage is properly regulated by frequency control [41]. This implies there is a tendency for the value of  $L_{mg}$  to be small and for a relatively large  $i_{Lmg}$  current to flow, even at no load, causing relatively large Joule loss. The LLC resonant

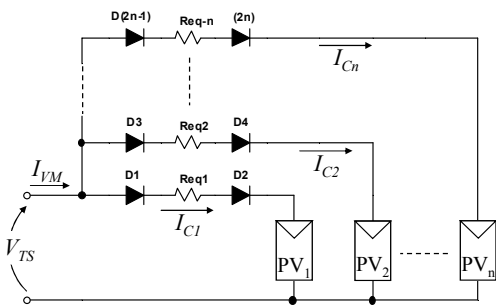


Fig. 8. DC equivalent circuit for voltage multiplier.

inverter in the proposed voltage equalizer, conversely, is operated at a fixed frequency, as mentioned in Section II-B, and used to drive the voltage multiplier to simply equalize voltages of series-connected PV modules. Therefore, the ratio of  $L_{mg}/L_r$  can be arbitrarily chosen without considering gain-frequency characteristic. To minimize the Joule loss at no load (i.e. that associated with  $i_{Lmg}$ ), the value of  $L_{mg}$  should be as large as  $L_{mg} \gg L_r$  to obtain the minimal value of  $i_{Lmg}$ , with which parasitic capacitances of MOSFETs,  $C_a$  and  $C_b$ , can still be sufficiently charged/discharged to recycle the stored energy in  $C_a$  and  $C_b$ .

To this end, the duty cycle needs to be properly determined. To simplify the analysis, it is assumed that  $i_{Lmg}$  in Modes 3 and 7 is constant and its value is  $\pm I_{Lmg-peak}$ , expressed as

$$I_{Lmg-peak} = \frac{N \left( \frac{1}{2} V_{PVi} + V_D \right) DT_S}{2L_{mg}}, \quad (8)$$

where  $D$  is the duty cycle of each switch. The time needed to fully charge/discharge  $C_a$  and  $C_b$ ,  $T_x$ , is yielded as

$$T_x = \frac{2C_{oss} V_{in}}{I_{Lmg-peak}} = \frac{8C_{oss} V_{String} L_{mg}}{N(V_{PVi} + 2V_D)DT_S}, \quad (9)$$

where  $C_{oss}$  is the capacitance of  $C_a$  and  $C_b$ . For  $C_a$  and  $C_b$  to be fully charged/discharged in Modes 3 and 7,  $D$  needs to be determined so that the length of Modes 3 and 7 exceeds  $T_x$ .

The voltage multiplier, including the transformer, can be replaced as an equivalent resistor,  $R_e$ ;

$$R_e = N^2 \frac{V_{m-TS}}{I_{m-VM}}. \quad (10)$$

The impedance of the resonant circuit is given by

$$Z_r = \frac{R_r + R_e(1+A) \left\{ 1 - \left( \frac{\omega_0}{\omega} \right)^2 \right\} + jZ_0 \left[ \left( \frac{\omega}{\omega_0} \right) \frac{A}{1+A} - \left( \frac{\omega_0}{\omega} \right) \left\{ 1 - \frac{R_r R_e}{Z_0^2} \right\} (1+A) \right]}{1 - j \frac{R_e}{Z_0} \left( \frac{\omega_0}{\omega} \right) (1+A)}, \quad (11)$$

where

$$\begin{cases} L = L_r + L_{mg}, & L_r = \frac{A}{1+A} L, & L_{mg} = \frac{1}{1+A} L \\ R_r = r_{DS} + r_r + r_{TP} + N^2 r_{TS} \end{cases}. \quad (12)$$

$r_{DS}$ ,  $r_r$ ,  $r_{TP}$ , and  $r_{TS}$  are the resistances of switches, resonant circuit and primary and secondary windings, respectively. From the FHA, the amplitude of  $i_{Lr}$ ,  $I_{m-Lr}$ , is expressed as

$$I_{m-Lr} = \frac{V_{m-String}}{|Z_r|}, \quad (13)$$

$$= V_{m-String} \sqrt{\frac{1 + \left\{ \frac{R_e}{Z_0} \left( \frac{\omega_0}{\omega} \right) (1+A) \right\}^2}{\left[ R_r + R_e(1+A) \left\{ 1 - \left( \frac{\omega_0}{\omega} \right)^2 \right\} \right]^2 + Z_0^2 \left[ \left( \frac{\omega}{\omega_0} \right) \frac{A}{1+A} - \left( \frac{\omega_0}{\omega} \right) \left\{ 1 - \frac{R_r R_e}{Z_0^2} \right\} (1+A) \right]^2}}$$

where  $V_{m-String}$  is the amplitude of the fundamental component of  $v_{DSb}$ , as designated in the inset of Fig. 9. Since the proposed voltage equalizer is designed to fulfill  $L_{mg} \gg L_r$  (i.e.  $A \approx 0$ ), and is therefore operated at  $\omega_r > \omega \gg \omega_0$ , (13) can be simplified as

$$I_{m-Lr} \approx \frac{V_{m-String}}{R_r + R_e} = \frac{V_{m-String} - NV_{m-TS}}{R_r} = \frac{2}{\pi} \frac{V_{String} - NV_{TS}}{R_r}. \quad (14)$$

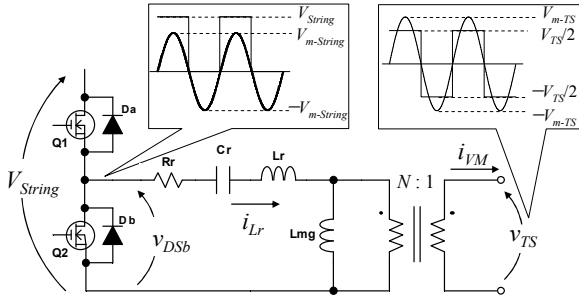


Fig. 9. Square voltage waves and approximated sinusoidal waves in LLC resonant inverter.

The average input current of the LLC resonant inverter,  $I_{in-ave}$ , can be yielded as

$$I_{in-ave} = \frac{1}{T_S} \int_0^{0.5T_S} I_{m-Lr} \sin \omega t dt = \frac{I_{m-Lr}}{\pi}. \quad (15)$$

Substituting (14) into (15) produces

$$V_{String} - NV_{TS} = I_{in-ave} R_{in}, \quad (16)$$

where

$$R_{in} = \frac{\pi^2}{2} R_r. \quad (17)$$

From (16), a dc equivalent circuit for the LLC resonant inverter can be derived as shown in Fig. 10.

#### D. Derivation for DC Equivalent Circuit

By combining the derived dc equivalent circuits for the voltage multiplier and LLC inverter shown in Figs. 8 and 10, a dc equivalent circuit of the proposed voltage equalizer as a whole is obtained, as shown in Fig. 11. For the modules of  $PV_1-PV_n$  to be connected in series, an ideal multi-winding transformer with a turn ratio of  $N:1:1:\dots:1$  is introduced.

The derived dc equivalent circuit reveals an intuitive understanding of how shaded PV modules in a string are supported by the proposed voltage equalizer. The string comprising  $PV_1-PV_n$  supplies power for the input in the form of  $I_{in-ave}$ , whereupon the supplied current is transferred to the secondary side in the form of  $I_{Ci}$ . Obviously,  $I_{Ci}$  preferentially flows toward the module with the lowest voltage, provided  $R_{eq-i}$  for each module is uniform. Under partially-shaded conditions,  $I_{Ci}$  is preferentially distributed to shaded modules because their voltages tend to be lower than those of unshaded modules when connected in series.

The characteristic of a PV string as a whole under a partially-shaded condition depends on the individual characteristics of series-connected PV modules, as mentioned in Section I, meaning each individual PV module and its characteristic should be included and taken into account for precise analysis. In general, a PV string is controlled by an MPPT converter that takes a relatively large sampling interval of several tens to hundreds milliseconds, whereas a voltage equalizer operates at a switching frequency exceeding a hundred kHz. This implies that, to grasp an MPPT performance under partially-shaded conditions by simulation analyses, long-time simulation at a high frequency is inevitable, resulting

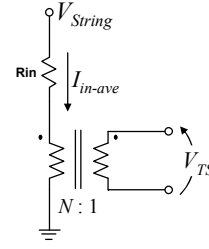


Fig. 10. DC equivalent circuit for LLC resonant inverter.

in increased burden of simulation. In addition, since a PV string comprises multiple modules connected in series, the burden of simulation using the original circuit operating at a high frequency is prone to increase with the number of series connections. This means the more series connections there are, the greater the number of components in a circuit, further complicating the circuitry and increasing the simulation burden. The derived dc equivalent circuit, conversely, is simpler and contains no high-frequency operation, which means the burden of simulation analysis would be considerably mitigated.

From the dc equivalent circuit,

$$V_{String} - I_{in-ave} R_{in} = N(V_{PV_i} + 2V_D + I_{Ci} R_{eq-i}). \quad (18)$$

$I_{in-ave}$  and  $V_{String}$  in the dc equivalent circuit can be expressed as

$$I_{in-ave} = \frac{\sum_i^n I_{Ci}}{N} = \frac{I_{Total}}{N}, \quad (19)$$

$$V_{String} = \sum_i^n V_{PV_i}. \quad (20)$$

When there is no shading, both  $I_{in-ave}$  and  $I_{Ci}$  should be zero so that the voltage equalizer consumes minimal power. By assuming  $V_{PV_i} \gg V_D$  and  $V_{String} = nV_{PV_i}$  under no-shading conditions, the following equation can be obtained for  $I_{in-ave}$  and  $I_{Ci}$  to be zero:

$$N = n. \quad (21)$$

By defining  $\alpha = I_{Ci}/I_{Total}$ , the output resistance for  $PV_i$ ,  $R_{out-i}$ ,

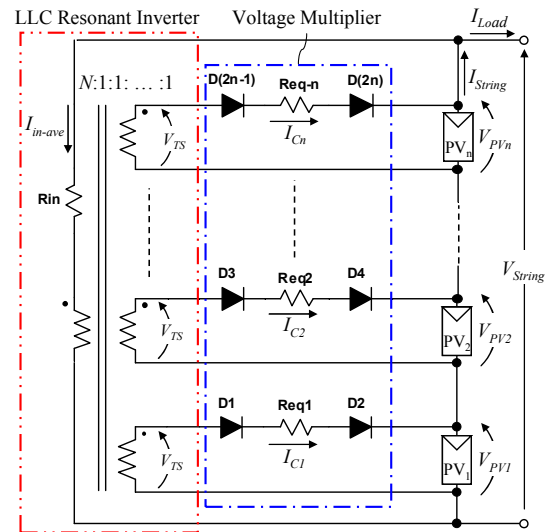


Fig. 11. DC equivalent circuit for proposed voltage equalizer.

can be yielded from (18) and (19), as

$$R_{out-i} = -\frac{\partial V_{PV_i}}{\partial I_{C_i}} = R_{eq-i} + \frac{R_{in}}{\alpha N^2}. \quad (22)$$

Here,  $\alpha = 1$  and  $\alpha < 1$  mean that one module ( $PV_i$ ) and multiple modules are shaded, respectively. Equation (22) implies that  $R_{out-i}$  depends on shading conditions. Where only one module is shaded ( $\alpha = 1$ ), the value of  $R_{out-i}$  is equal to  $R_{eq-i} + R_{in}/N^2$ . Meanwhile, if more than two modules are shaded at a time ( $\alpha < 1$ ),  $R_{out-i}$  depends on  $\alpha$ , meaning that  $R_{out-i}$  for each module is influenced by other modules' shaded conditions. This can be better understood with the derived dc equivalent circuit;  $R_{eq-i}$  is connected to each module, whereas  $R_{in}$  acts as a common resistor, and therefore,  $R_{out-i}$  for each module is mutually dependent.

#### E. Consideration for Impact of Parameter Mismatch

The derived dc equivalent circuit shown in Fig. 11 and (18) imply that parameter mismatch in  $V_D$  and  $R_{eq-i}$  would result in nonuniform  $V_{PV_i}$ ; the value of  $V_{PV_i}$  is dependent on  $V_D$  and  $I_{C_i}R_{eq-i}$ . Since the equalizer is designed so that  $I_{C_i}$  flows toward shaded modules only, as mentioned in the previous subsection, the parameter mismatch would be an issue in the case that multiple PV modules are simultaneously shaded.

The impact of parameter mismatch on overall power utilization of the string as a whole would be beneficial or detrimental depending on various conditions because shaded modules might fortunately operate at its MPP thanks to the nonuniform  $V_{PV_i}$ . Thus, detailed investigation including case study is considered indispensable that would be a part of our future works.

In this paper, we assumed that minimizing the parameter mismatch is a reasonable design. Equation (18) suggests that the impact of the parameter mismatch would be negligible, if the voltage equalizer is designed so that  $V_D$  and  $I_{C_i}R_{eq-i}$  are negligibly small compared to  $V_{PV_i}$ . In other words, it is advised that the voltage equalizer is designed to satisfy  $V_{PV_i} \gg V_D$  and  $V_{PV_i} \gg I_{C_i}R_{eq-i}$  in order to minimize the impact of parameter mismatch.

#### IV. POWER DISTRIBUTION SCENARIO UNDER PARTIALLY-SHADED CONDITION

As (18) implies, a voltage of shaded modules is dependent on how much current is supplied from the equalizer. For the sake of simplicity, it is assumed that all module voltages are ideally unified by the equalizer, and unshaded modules receive no current from the equalizer; this ideal condition corresponds to the dc equivalent circuit (Fig. 11) with  $R_{in} = 0$ ,  $V_D = 0$ , and  $R_{eq-i} = 0$ .

Power distribution under the case that  $PV_1$ – $PV_3$  are partially-shaded is considered as an example (Fig. 12);  $PV_1$ – $PV_4$  are assumed to be able to generate 5, 10, 30, and 50 W, respectively. Since all the modules in the string are subjected to the same string current and the voltage equalizer operates so that all the module voltages are unified, shaded modules of  $PV_1$ – $PV_3$  receive differential powers of 45, 40, and 20 W, respectively,

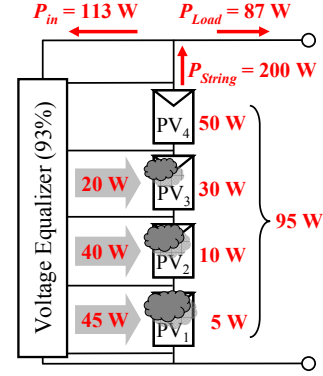


Fig. 12. Example of power distribution scenario under severe partial-shading condition.

from the equalizer. If the power conversion efficiency of the voltage equalizer is 93%, the equalizer requires an input power of 113 W that is larger than the total generated power of 95 W. However, with the support of the equalizer, the string is virtually able to produce 200 W, and consequently, 87 W is provided for a load. In other words, the voltage equalizer operates as a power circulator, and redistributes the power to shaded modules.

Although the above example was a severely-shaded condition—the processed power in the voltage equalizer is larger than the power supplied to the load—, power circulation and distribution take place in the similar manner under any partially-shaded conditions. For more detailed analysis, the derived dc equivalent circuit (Fig. 11) would be a powerful tool that can incorporate non-ideal conditions.

#### V. LOSS ANALYSIS

##### A. LLC Resonant Inverter

The switches are turned-on at ZVZCS and -off at ZVS as mentioned in Section III-A, meaning losses in the LLC resonant inverter can be modeled without considering switching losses. Since the proposed voltage equalizer is designed with  $L_{mg} \gg L_r$  to minimize  $i_{Lmg}$  as mentioned in Section III-C,  $i_{Lr} = i_{VM}/N$  can be assumed. The transformer iron loss is modeled conventionally as [42], while the Joule loss in the LLC resonant inverter,  $P_{Loss-Resonant}$ , can be expressed as

$$P_{Loss-Resonant} = \frac{2}{T_S} \int_0^{0.5T_r} R_r I_{m-Lr}^2 \sin \omega_r t dt = \frac{\omega_r}{\omega} \frac{\pi^2 R_r I_{VM}^2}{2N^2}. \quad (23)$$

##### B. Voltage Multiplier

Losses in the voltage multiplier depend on how many modules are shaded. In this subsection, losses associated with each shaded module are separately modeled.

The conduction loss in a diode,  $P_{Loss-D}$ , is expressed as

$$P_{Loss-D} = \frac{1}{T_S} \int_0^{0.5T_r} V_D I_{m-Ci} \sin \omega_r t dt = V_D I_{C_i}. \quad (24)$$

The Joule loss in  $C_i$  is

$$P_{Loss-Ci} = \frac{2}{T_S} \int_0^{0.5T_r} r_{C_i} I_{m-Ci}^2 \sin \omega_r t dt = \frac{\omega_r}{\omega} \frac{\pi^2 r_{C_i} I_{C_i}^2}{2}. \quad (25)$$

The modeling for Joule loss in smoothing capacitors is



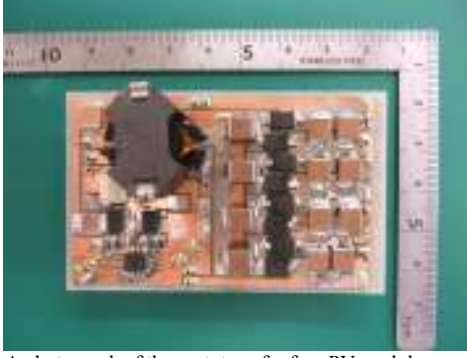


Fig. 13. A photograph of the prototype for four PV modules connected in series.

somewhat elusive because the number of smoothing capacitors subject to current flow depends on shading conditions as well as the number of PV modules connected in series. For example, if only one module of  $PV_1$  is shaded as shown in Fig. 6, currents from the equalizer flow through not only  $C_{out1}$  but also  $C_{out2}$  (though the average current supplied to  $PV_2$  is zero), causing Joule losses in both  $C_{out1}$  and  $C_{out2}$ . Accordingly, the Joule loss in smoothing capacitors needs to be modeled considering specific current paths. Here, the loss in smoothing capacitors is modeled by taking an example of the case shown in Fig. 6 — only  $PV_1$  is shaded.

The current of  $C_{out1}$ ,  $i_{Cout1}$ , is modeled as a dc current of  $I_{C1}$  on which an ac current of  $i_{C1} = I_{m-C1} \sin \omega_r t$  is superimposed, whereas the current of  $C_{out2}$ ,  $i_{Cout2}$ , is equal to  $i_{C1}$ ;

$$i_{Cout1} = \begin{cases} I_{m-C1} \sin \omega_r t - I_{C1} & (0 < t < 0.5T_r) \\ -I_{C1} & (0.5T_r < t < T_s) \end{cases} \quad (26)$$

$$i_{Cout2} = i_{C1} \quad (27)$$

Table I. Component values.

Component	Value
$C_1$ – $C_4$	Ceramic Capacitor, 94 $\mu$ F, 10 m $\Omega$
$C_{out1}$ – $C_{out4}$	Ceramic Capacitor, 188 $\mu$ F, 10 m $\Omega$
$D_1$ – $D_8$	Schottky Diode, CLS01, $V_D = 0.47$ V, $R_D = 20$ m $\Omega$
$C_r$	Film Capacitor, 330 nF, 135 m $\Omega$
Transformer	$N_1 : N_2 = 12:3$ , $L_{kg} = 0.95$ $\mu$ H, $L_{mg} = 85$ $\mu$ H $r_{TP} = 140$ m $\Omega$ , $r_{TS} = 11.2$ m $\Omega$
$Q_a, Q_b$	N-Ch MOSFET, FDS86240, $R_{on} = 35.3$ m $\Omega$

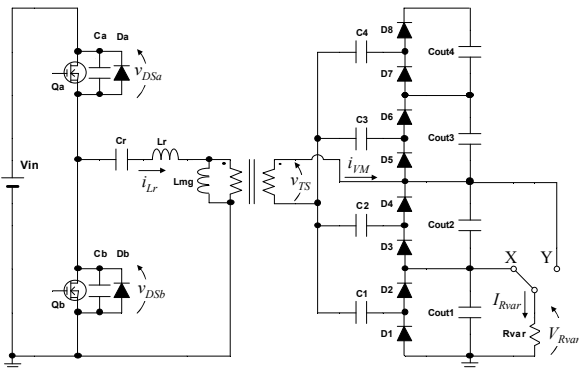


Fig. 14. Experimental setup for efficiency and output characteristic measurement.

The Joule losses in  $C_{out1}$  and  $C_{out2}$  are

$$P_{Loss-Cout1} = \frac{1}{T_S} \int_0^{T_S} r_{Cout1} i_{Cout1}^2 dt = r_{Cout1} I_{C1}^2 \left( \frac{\omega_r \pi^2}{\omega} - 1 \right), \quad (28)$$

$$P_{Loss-Cout2} = \frac{1}{T_S} \int_0^{T_S} r_{Cout2} i_{Cout2}^2 dt = \frac{\omega_r}{\omega} \frac{\pi^2 r_{Cout2} I_{C1}^2}{2}. \quad (29)$$

## VI. EXPERIMENTAL RESULTS

### A. Prototype and Experimental Setup

A prototype that can supply 50 W for each shaded module — it can be regarded equivalent to four 50-W converters — was built on a single-sided PCB for four PV modules connected in series, as shown in Fig. 13. Component values are listed in Table I. The prototype was operated at a fixed switching frequency of 200 kHz with  $D = 0.44$ ; although the higher switching frequency contribute to size reduction, the moderate frequency of 200 kHz was chosen to keep the no-load loss at a reasonable level. The efficiency measurement was performed using the experimental setup shown in Fig. 14.  $PV_1$ – $PV_4$  were removed and the prototype was powered by an external power source  $V_{in}$ , while a variable resistor  $R_{var}$  was used to emulate current paths under partially-shaded conditions; one-module-shaded condition ( $PV_1$  shaded) can be emulated by selecting the tap X, while the tap Y emulates the condition where two modules of  $PV_1$  and  $PV_2$  are

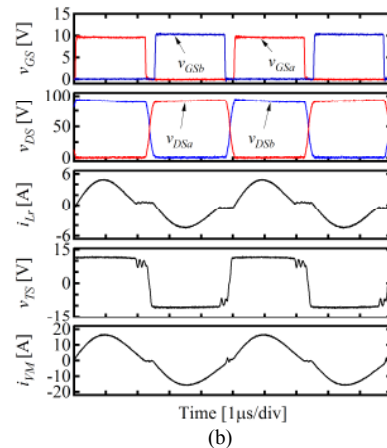
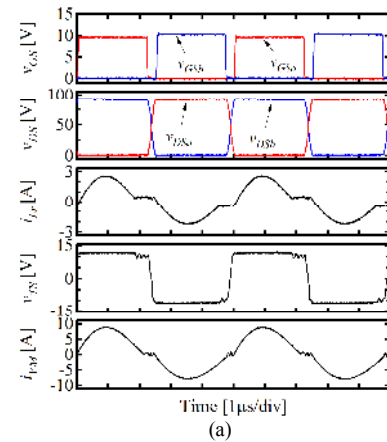


Fig. 15. Measured key waveforms at  $I_{Rvar} = 2.5$  A under (a) one- and (b) two-module-shaded conditions.

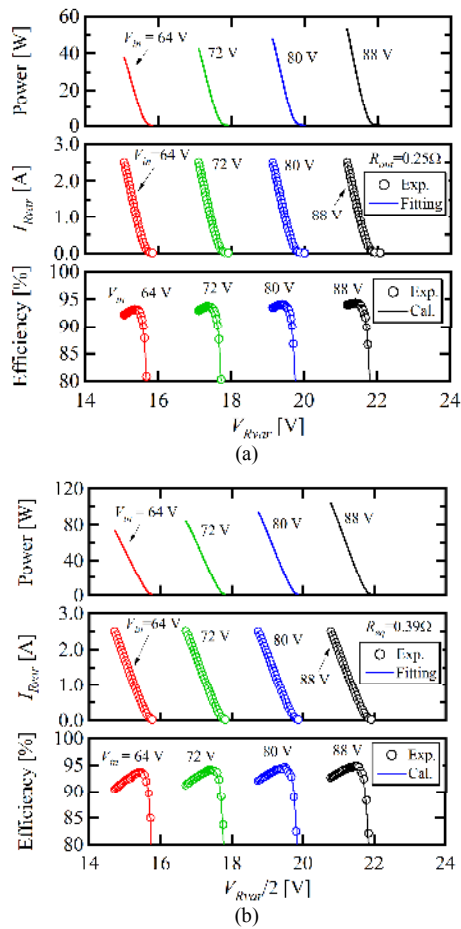


Fig. 16. Measured power conversion efficiencies and output characteristics under (a) one- and (b) two-module-shaded conditions.

equally shaded. Power conversion efficiencies as well as output characteristics were measured at various input voltages of  $V_{in} = 64\text{--}88\text{ V}$  that correspond to each module voltage of  $16\text{--}22\text{ V}$  in a practical case —  $V_{in}$  corresponds to the sum of voltages of four modules  $V_{PV1}\text{--}V_{PV4}$  in a practical case.

### B. Fundamental Performance

Measured key waveforms at  $V_{in} = 88\text{ V}$  and  $I_{Rvar} = 2.5\text{ A}$  under one- and two-module-shaded conditions are shown and compared in Fig. 15. Waveforms under both conditions agreed well with the theoretical ones shown in Fig. 5. Amplitudes of  $i_{Lr}$  and  $i_{VM}$  under the two-module-shaded condition were double those under the one-module-shaded condition because the processed power was also double.

The measured power conversion efficiencies and output characteristics under one- and two-module-shaded conditions are shown in Fig. 16. The measured output currents increased almost linearly as  $V_{Rvar}$  decreased. Similar to ordinary converters, measured efficiencies declined and approached 0% as the output powers decreased at light load conditions, whereby the no-load losses, such as the iron and gate driving losses, dominated: the estimated loss breakdown will be shown in Fig. 17. From the slopes of the measured current characteristics, the values of  $R_{out}$  under one- and two-module-shaded conditions were determined as approximately  $0.25$  and  $0.39\ \Omega$ ,

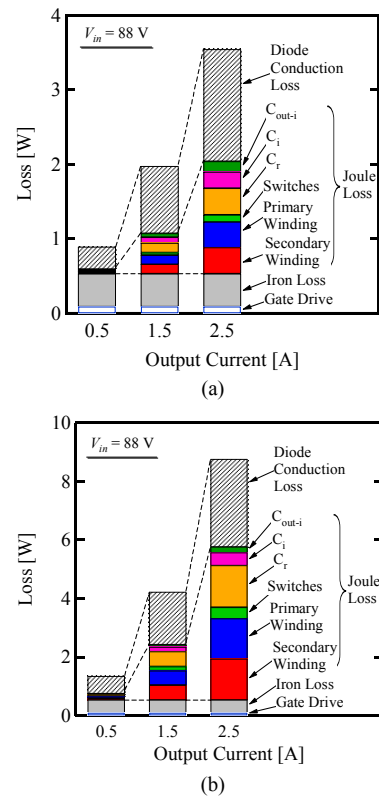


Fig. 17. Estimated loss breakdown at  $V_{in} = 88\text{ V}$  under (a) one- and (b) two-module-shaded conditions.

respectively, based on which values of  $R_{in}$  and  $R_{eq-i}$  were also determined as  $2.24$  and  $0.11\ \Omega$ , respectively, according to (22). Experimental and calculated efficiencies based on losses modeled in Section V matched well, and measured peak efficiencies were as high as 93–95%. These measured efficiencies may look inferior to those of the DPP converters (for example [5]). However, given that the direct power transfer to shaded modules is feasible with the proposed equalizer as discussed in Section II-B, a practical overall efficiency would be higher or lower, depending on partial-shading conditions and the number of modules connected in series. Detailed analysis including case study should be performed in future works to fairly compare different architectures.

Estimated loss breakdowns at  $V_{in} = 88\text{ V}$  under one- and two-module-shaded conditions are shown in Fig. 17. From the measured no-load loss, the iron and gate driving losses were determined as  $0.44$  and  $0.09\text{ W}$ , respectively, while the diode conduction loss was the most dominant factor at output currents of  $1.5$  and  $2.5\text{ A}$ . The Joule losses in the LLC resonant inverter (i.e. switches,  $C_r$ , and transformer windings) under the two-module-shaded condition accounted for a greater ratio than those under the one-module-shaded condition due to the double value of  $i_{Lr}$  and  $i_{VM}$  under the two-module-shaded condition, as shown in Fig. 15.

### C. Experimental Equalization Emulating Partially-Shaded Conditions

Experimental equalization tests were performed emulating partially-shaded conditions. Solar Array Simulators (E4350B,

Agilent Technology) were used to emulate arbitrary characteristics of PV modules under partially-shaded conditions. Individual PV characteristics were generated by specifying four model parameters: open-circuit voltage, short-circuit current, and voltage and current at the MPP. Voltage and current values at the MPP and open- and short-circuit conditions are designated in Fig. 18(a). A bypass diode was also connected to each module to compare string characteristics with/without equalization.

The first experimental equalization test was performed emulating the PV<sub>1</sub>-shaded condition; the individual PV characteristics used for the first experiment are shown in Fig. 18(a). The measured individual PV characteristics with equalization are shown in Fig. 18(b), in which the virtual PV<sub>1</sub> characteristic (i.e. the PV<sub>1</sub> characteristic supported by the equalizer) is designated as PV<sub>1</sub> (w/ Eq). When the string current  $I_{String}$  was 2.85 A, for example, the unshaded modules of PV<sub>2</sub>–PV<sub>4</sub> were operated at point A, their MPP. Meanwhile, the operating point of PV<sub>1</sub> was C. Since all modules in a string are subject to the same current, the equalizer supported the shaded module of PV<sub>1</sub> by supplying current corresponding to the difference between A and C (approximately 1.0 A) so that the

sum of the generated current of PV<sub>1</sub> (1.85 A at point C) and the current supported by the equalizer was 2.85 A. Thus, the virtual operating point of PV<sub>1</sub> with equalization was determined as B, at which the operating voltage and current were equivalent to those of PV<sub>1</sub> and PV<sub>2</sub>–PV<sub>4</sub>, respectively. These operating points can be determined based on (18), and hence readily estimated based on simulation analysis using the derived dc equivalent circuit illustrated in Fig. 12, as will be shown in the next subsection.

The measured string characteristics with/without equalization are compared in Fig. 18(c). Two MPPs (global and local) were observed and the extractable maximum power was about 150 W without equalization. With equalization, conversely, the local MPP disappeared and extractable maximum power increased to as much as 185 W, demonstrating the effectiveness of the proposed voltage equalizer. The theoretical extractable maximum power in the first experimental condition was 187.3 W—if all modules could ideally operate at each MPP—, meaning 98.8% of the theoretical string power was extractable with the proposed voltage equalizer. Although the individual MPPT is unfeasible with the proposed equalizer and the peak efficiencies were 93–95% (Fig. 16), most of the theoretical

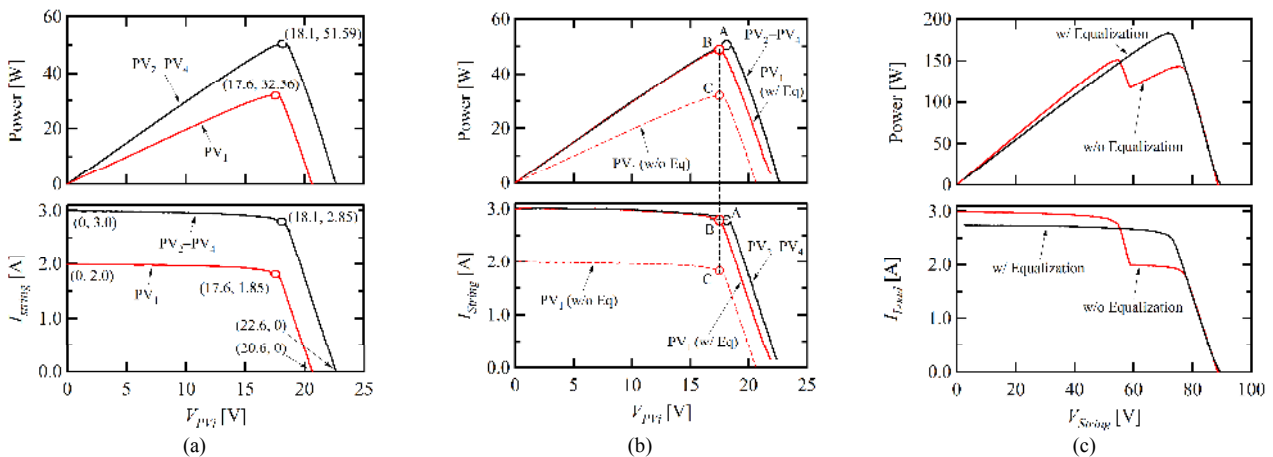


Fig. 18. Experimental results of the first equalization test; (a) individual PV characteristics used for the experiment, (b) individual PV characteristics with equalization, and (c) string characteristics with/without equalization.

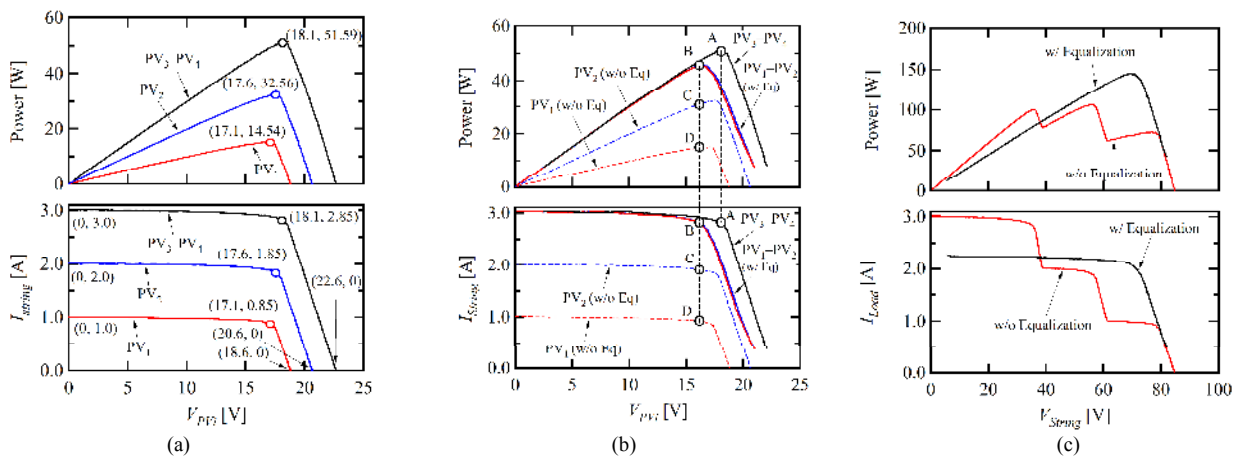


Fig. 19. Experimental results of the second equalization test; (a) individual PV characteristics used the experiment, (b) individual PV characteristics with equalization, and (c) string characteristics with/without equalization.

maximum power was extractable because the shaded module of  $PV_1$  was able to operate at a near-MPP (point C in Fig. 18(b)) and the processed power in the equalizer was only about 17 W (the difference between B and C in the upper panel in Fig. 18(b)).

The second experimental equalization was performed emulating the partially-shaded condition where  $PV_1$  and  $PV_2$  are severely and moderately shaded, respectively. Individual PV characteristics used for the second experiment are shown in Fig. 19(a). The measured individual PV characteristics with equalization are shown in Fig. 19(b) and the operating point of each PV module can be determined similarly as explained earlier for the first experiment. When  $I_{String}$  was 2.85 A, the operating points of  $PV_3$  and  $PV_4$  were at A, while the shaded modules of  $PV_1$  and  $PV_2$  operated at nearly the same voltage of 16 V and their respective operating points were D and C, respectively. The voltage equalizer supported currents corresponding to A – D and A – C for  $PV_1$  and  $PV_2$ , respectively, so that all the modules would be subject to the same current of 2.85 A, and the virtual operating point of  $PV_1$  and  $PV_2$  was determined as B. According to (18), the larger the current supported by the equalizer, the lower the operating

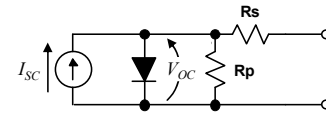


Fig. 20. Equivalent circuit for PV module.

voltage of the shaded modules will be due to the voltage drop in  $R_{eq-i}$ . Although the current supported for  $PV_1$  from the equalizer was almost double that for  $PV_2$ , the measured virtual characteristics of  $PV_1$  and  $PV_2$  were nearly the same, thanks to the low resistance value of  $R_{eq-i} = 0.11 \Omega$ , as determined in the previous subsection.

The measured string characteristics with/without equalization are compared in Fig. 19(c). Multiple MPPs found under the no-equalization condition successfully converged under the equalized condition. The extractable maximum power was significantly increased from 105 to 145 W by the equalizer, demonstrating that the proposed voltage equalizer can also support multiple shaded PV modules. The theoretical extractable maximum power in the second experiment was 150.3 W, and thus 96.5% of the potential string power was extractable with the proposed equalizer. This value is somewhat

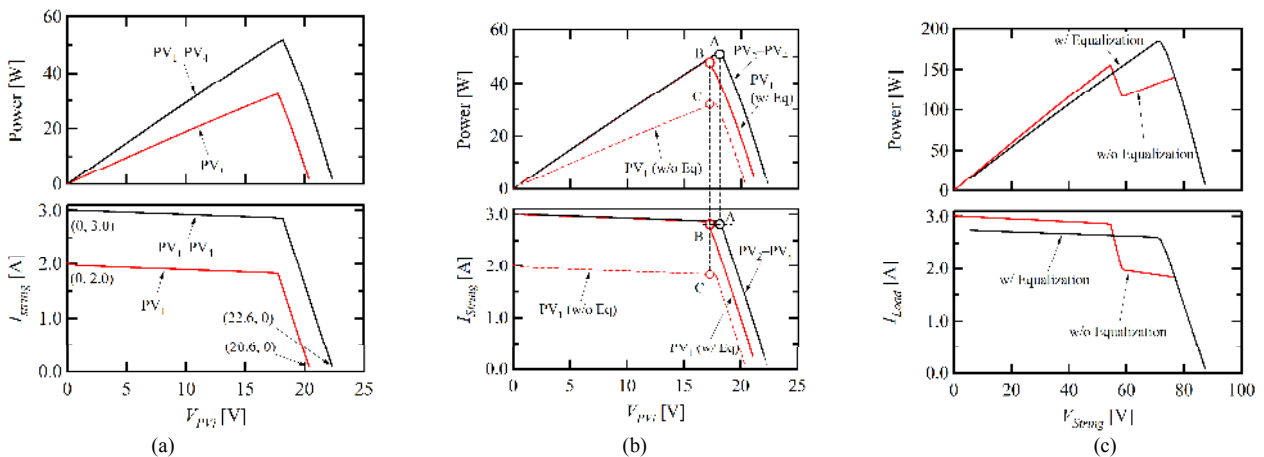


Fig. 21. Results of simulation analysis emulating the first equalization experiment; (a) individual PV characteristics used for simulation, (b) individual PV characteristics with equalization, and (c) string characteristics with/without equalization.

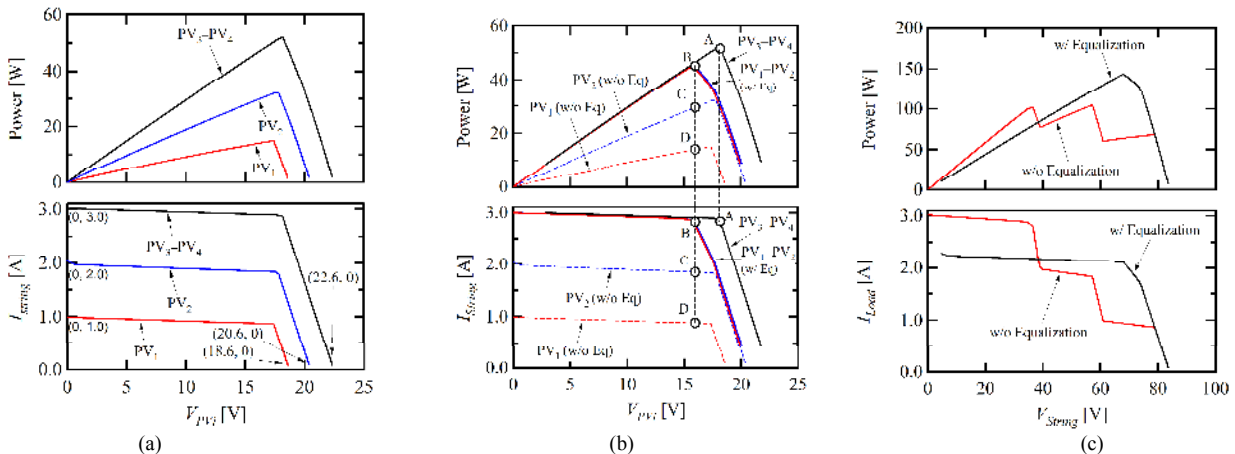


Fig. 22. Results of simulation analysis emulating the second equalization experiment; (a) individual PV characteristics used for simulation, (b) individual PV characteristics with equalization, and (c) string characteristics with/without equalization.

inferior to that in the first experiment and is attributable to the increased processed power as well as the lowered utilization of shaded modules—points C and D in Fig. 19(b) are slightly far from each MPP compared to the case in Fig. 18(b).

#### D. Simulation Results of the Derived DC Equivalent Circuit

Simulation analyses using the derived dc equivalent circuit shown in Fig. 11 were also performed emulating the same partially-shaded conditions as the experiments. A simple equivalent circuit model for the PV module shown in Fig. 20 was used for the simulation analyses;  $I_{SC}$  and  $V_{OC}$  are the short-circuit current and open-circuit voltage, respectively, while  $R_s$  and  $R_p$  are series and parallel resistances with values chosen as 1.5 and 120  $\Omega$ , respectively, to imitate the PV characteristics used in the experiment. The values of  $R_{in}$  and  $R_{eq-i}$  were 2.24 and 0.11  $\Omega$ , respectively, as determined from the results shown in Fig. 16 in Section VI-B.

The results of the simulation analyses emulating the first and second experimental conditions are shown in Figs. 21 and 22, respectively. These results match well with the experimental results shown in Figs. 18 and 19, verifying the derived dc equivalent circuit.

## VII. CONCLUSIONS

A two-switch voltage equalizer using an LLC resonant inverter with a voltage multiplier has been proposed in this paper. The two-switch configuration can significantly simplify the circuitry compared with conventional topologies of DPP converters and voltage equalizers requiring multiple switches proportional to the number of PV modules connected in series. In addition, the proposed voltage equalizer operates with open-loop control, further simplifying the circuitry by eliminating feedback control loop and circuit.

Operation analyses for the LLC resonant inverter and voltage multiplier were separately performed and their dc equivalent circuits were derived based on mathematical analyses. By combining these derived circuits, a dc equivalent circuit of the voltage equalizer as a whole, with which a PV string, including the voltage equalizer, can be modeled very simply and the burden of simulation analyses can be considerably mitigated, was also derived.

Experimental equalization tests using the prototype of the proposed voltage equalizer were performed for four PV modules connected in series, emulating partially-shaded conditions. With the proposed voltage equalizer, local MPPs successfully disappeared and extractable maximum powers significantly increased compared with those without equalization. Simulation analyses using the derived dc equivalent circuit were also performed emulating the same partially-shaded condition as the experiments. The simulation and experimental results matched well, verifying the analysis as well as the derived dc equivalent circuit.

## REFERENCES

[1] S. Poshtkouhi, V. Palaniappan, M. Fard, and O. Trescases, "A general approach for quantifying the benefit of distributed power electronics for

fine grained MPPT in photovoltaic applications using 3-D modeling," *IEEE Trans. Power Electron.*, vol. 27, no. 11, pp. 4656–4666, Nov. 2012.

[2] M. Vitelli, "On the necessity of joint adoption of both distributed maximum power point tracking and central maximum power point tracking in PV systems," *Prog. Photovolt. Res. Appl.*, vol. 22, pp. 283–299, 2014.

[3] P. S. Shenoy, K. A. Kim, B. B. Johnson, and P. T. Krein, "Differential power processing for increased energy production and reliability of photovoltaic systems," *IEEE Trans. Ind. Power Electron.*, vol. 28, no. 6, pp. 2968–2979, Jun. 2013.

[4] H. J. Bergveld, D. B uthker, C. Castello, T. Doorn, A. D. Jong, R. V. Otten, and K. D. Waal, "Module-level DC/DC conversion for photovoltaic systems: the delta-conversion concept," *IEEE Trans. Power Electron.*, vol. 28, no. 4, pp. 2005–2013, Apr. 2013.

[5] S. Qin and R. C. N. P. Podgurski, "Sub-module differential power processing for photovoltaic applications," in *Proc. IEEE Applied Power Electron. Conf. Expo.*, pp. 101–108, 2013.

[6] S. Qin, S. T. Cady, A. D. D. Garc a, and R. C. N. P. Podgurski, "A distributed approach to MPPT for PV sub-module differential power processing," in *Proc. IEEE Energy Conversion Conf. Expo.*, pp. 2778–2785, 2013.

[7] R. Kadri, J. P. Gaubert, and G. Champenois, "New converter topology to improve performance of photovoltaic power generation system under shading conditions," in *Proc. Int. Conf. Power Eng. Energy Electrocal Drives*, pp. 1–7, 2011.

[8] R. Kadri, J. P. Gaubert, and G. Champenois, "Centralized MPPT with string current diverter for solving the series connection problem in photovoltaic power generation system," in *Proc. Int. Conf. Power Eng. Energy Electrocal Drives*, pp. 116–123, 2011.

[9] R. Giral, C. A. R. Paja, D. Gonzalez, J. Calvente,  . C. Pastpr, and L. M. Salamero, "Minimizing the effects of shadowing in a PV module by means of active voltage sharing," in *Proc. IEEE Int. Conf. Ind. Technol.*, pp. 943–948, 2010.

[10] R. Giral, C. E. Carrejo, M. Vermeersh, A. J. Saavedra-Montes, and C. A. Ramos-Paja, "PV field distributed maximum power point tracking by means of an active bypass converter," in *Proc. Int. Conf. Clean Electrical Power*, pp. 94–98, 2011.

[11] L. F. L. Villa, T. P. Ho, J. C. Crebier, and B. Raison, "A power electronics equalizer application for partially shaded photovoltaic modules," *IEEE Trans. Ind. Electron.*, vol. 60, no. 3, pp. 1179–1190, Mar. 2013.

[12] L. F. L. Villa, X. Pichon, F. S. Ardelibi, B. Raison, J. C. Crebier, and A. Labonne, "Toward the design of control algorithms for a photovoltaic equalizer: choosing the optimal switching strategy and the duty cycle," *IEEE Power Electron.*, vol. 29, no. 3, pp. 1447–1460, Mar. 2014.

[13] Z. Salam and M. Z. Ramli, "A simple circuit to improve the power yield of PV array during partial shading," in *Proc. IEEE Energy Conversion Cong. Expo.*, pp. 1622–1626, 2012.

[14] S. Poshtkouhi, A. Biswas, O. Trescases, "Dc-dc converter for high granularity sub-string MPPT in photovoltaic applications using a virtual-parallel connection," in *Proc. IEEE Applied Power Electron. Conf. Expo.*, pp. 86–92, 2012.

[15] T. Shimizu, O. Hashimoto, and G. Kimura, "A novel high-performance utility-interactive photovoltaic inverter system," *IEEE Trans. Power Electron.*, vol. 18, no. 2, pp. 704–711, Mar. 2003.

[16] T. Shimizu, M. Hirakata, T. Kamezawa, and H. Watanabe, "Generation control circuit for photovoltaic modules," *IEEE Trans. Power Electron.*, vol. 16, no. 3, pp. 293–300, May 2001.

[17] J. T. Stauth, M. D. Seeman, and K. Kesarwani, "Resonant switched-capacitor converters for sub-module distributed photovoltaic power management," *IEEE Trans. Power Electron.*, vol. 28, no. 3, pp. 1189–1198, Mar. 2013.

[18] S. B. Yaakov, A. Blumenfeld, A. Cervera, and M. Evzelman, "Design and evaluation of a modular resonant switched capacitor equalizer for PV panels," in *Proc. IEEE Energy Conversion Cong. Expo.*, pp. 4129–4136, 2012.

[19] Y. Nimni and D. Shmilovitz, "Returned energy architecture for improved photovoltaic systems efficiency," in *Proc. IEEE Int. Symp. Circuit Syst.*, pp. 2191–2194, 2010.

[20] C. Olalla, M. Rodr guez, D. Clement, J. Wang, and D. Makisimovi c, "Architecture and control of PV modules with submodule integrated

- converter,” in *Proc. IEEE Control and Modeling for Power Electron.*, pp. 1–6, 2012.
- [21] C. Olalla, D. Clement, M. Rodríguez, and D. Maksimović, “Architectures and control of submodule integrated dc-dc converters for photovoltaic applications,” *IEEE Trans. Power Electron.*, vol. 28, no. 6, pp. 2980–2997, Jun. 2013.
- [22] C. Olalla, C. Deline, D. Clement, Y. Levron, M. Rodríguez, and D. Maksimović, “Performance of power limited differential power processing architectures in mismatched PV systems,” *IEEE Trans. Power Electron.*, to be published.
- [23] Q. Zhang, X. Sun, Y. Zhong, and M. Matui, “A novel topology for solving the partial shading problem in photovoltaic power generation system,” in *Proc. IEEE Power Electron. Motion Cont. Conf.*, pp. 2130–2135, 2009.
- [24] J. Du, R. Xu, X. Chen, Y. Li, and J. Wu, “A novel solar panel optimizer with self-compensation for partial shadow condition,” in *Proc. IEEE Applied Power Electron. Conf. Expo.*, pp. 92–96, 2013.
- [25] K. Nishijima, H. Sakamoto, and K. Harada, “A PWM controlled simple and high performance battery balancing system,” in *Proc. IEEE Power Electron. Spec. Conf.*, Jun. 2000, pp. 517–520.
- [26] T. H. Phung, A. Collet, and J. Crebier, “An optimized topology for next-to-next balancing of series-connected lithium-ion cells,” *IEEE Trans. Power Electron.*, vol. 29, no. 9, Sep. 2014, pp. 4603–4613.
- [27] P. A. Cassani and S. S. Williamson, “Feasibility analysis of a novel cell equalizer topology for plug-in hybrid electric vehicle energy-storage systems,” *IEEE Trans. Veh. Technol.*, vol. 58, no. 8, Oct. 2009, pp. 3938–3946.
- [28] P. A. Cassani and S. S. Williamson, “Design, testing, and validation of a simplified control scheme for a novel plug-ion hybrid electric vehicle battery cell equalizer,” *IEEE Trans. Ind. Electron.*, vol. 57, no. 12, Dec. 2010, pp. 3956–3962.
- [29] J. W. Kimball, B. T. Kuhn, and P. T. Krein, “Increased performance of battery packs by active equalization,” in *Proc. IEEE Veh. Power Propulsion Conf.*, Sep. 2007, pp. 323–327.
- [30] A. Baughman and M. Ferdowsi, “Double-tiered switched-capacitor battery charge equalization technique,” *IEEE Trans. Ind. Appl.*, vol. 55, no. 6, Jun. 2008, pp. 2277–2285.
- [31] M. Uno and K. Tanaka, “Influence of high-frequency charge-discharge cycling induced by cell-voltage equalizers on the life performance of lithium-ion cells,” *IEEE Trans. Veh. Technol.*, vol. 60, no. 4, May 2011, pp. 1505–1515.
- [32] Y. Yuanmao, K. W. E. Cheng, and Y. P. B. Yeung, “Zero-current switching switched-capacitor zero-voltage-gap automatic equalization system for series battery string,” *IEEE Trans. Power Electron.*, vol. 27, no. 7, Jul. 2012, pp. 3234–3242.
- [33] M. Y. Kim, C. H. Kim, J. H. Kim, and G. W. Moon, “A chain structure of switched capacitor for improved cell balancing speed of lithium-ion batteries,” *IEEE Trans. Ind. Electron.*, vol. 61, no. 9, Aug. 2014, pp. 3989–3999.
- [34] H. S. Park, C. E. Kim, C. H. Kim, G. W. Moon, and J. H. Lee, “A modularized charge equalizer for an HEV lithium-ion battery string,” *IEEE Trans. Ind. Electron.*, vol. 56, no. 5, May 2009, pp. 1464–1476.
- [35] C. H. Kim, H. S. Park, C. E. Kim, G. W. Moon, and J. H. Lee, “Individual charge equalization converter with parallel primary winding of transformer for series connected lithium-ion battery strings in an HEV,” *J. Power Electron.*, vol. 9, no. 3, May 2009, pp. 472–480.
- [36] N. H. Kutkut, D. M. Divan, and D. W. Novotny, “Charge equalization for series connected battery strings,” *IEEE Trans. Ind. Appl.*, vol. 31, no. 3, May/June 1995, pp. 562–568.
- [37] N. H. Kutkut, H. L. N. Wiegman, D. M. Divan, and D. W. Novotny, “Charge equalization for an electric vehicle battery system,” *IEEE Trans. Aerosp. Electron. Syst.*, vol. 34, no. 1, Jan. 1998, pp. 235–246.
- [38] N. H. Kutkut, H. L. N. Wiegman, D. M. Divan, and D. W. Novotny, “Design considerations for charge equalization of an electric vehicle battery system,” *IEEE Trans. Ind. Appl.*, vol. 35, no. 1, Jan. 1999, pp. 28–35.
- [39] J. Cao, N. Schofield, and A. Emadi, “Battery balancing methods: a comprehensive review,” in *Proc. IEEE Veh. Power Propulsion Conf.*, Sep. 2008, pp. 1–6.
- [40] K. Z. Guo, Z. C. Bo, L. R. Gui, and C. S. Kang, “Comparison and evaluation of charge equalization technique for series connected batteries,” in *Proc. IEEE Power Electron. Spec. Conf.*, Jun. 2006, pp. 1–6.

- [41] H. Choi, “Desing consideration for an LLC-resonant converter,” Fairchild Power Seminar 2007. <http://www.fairchildsemi.co.jp/Assets/zSystem/documents/collateral/onlineSeminars/Design-Considerations-for-an-LLC-Resonant-Converter-WP.pdf>
- [42] A. V. D. Bossche and V. C. Valchev, *Inductors and transformers for power electronics*, Boca Raton: CRC Press, 2005, ch. 3.



**Masatoshi Uno** (M’06) was born in Japan in 1979. He received the B.E. degree in electronics engineering and the M.E. degree in electrical engineering from Doshisha University, Kyoto, Japan, in 2002 and 2004, respectively, and the Ph.D degree from the Graduate University for Advanced Studies, Kanagawa, Japan, in 2012.

Since 2004, he has been with Japan Aerospace Exploration Agency where he is currently a development researcher for spacecraft power systems.

His research areas include switching power converters, cell equalizers, and life evaluation for supercapacitors and lithium-ion batteries, and development of fuel cell systems, for spacecraft power systems.

M. Uno is a member of the Institute of Electrical Engineering of Japan (IEEJ), and the Institute of Electronics, Information and Communication Engineers (IEICE).



**Akio Kukita** was born in Japan in 1967. He received the B.E. degree in physics from Chuo University, Japan, in 1993.

From 1993 to 1996 and 1996 to 2008, he was with SEIKO Holdings Corporation and Ebara Corporation, respectively. Since 2008, he has been with Japan Aerospace Exploration Agency as a senior engineer. His recent work has focused on the development of spacecraft power systems.